Bedrock incision, rock uplift and threshold hillslopes in the northwestern Himalayas

Douglas W. Burbank*, John Leland†, Eric Fielding‡, Robert S. Anderson§, Nicholas Brozovic*, Mary R. Reid† & Christopher Duncan||

* Department of Earth Sciences, University of Southern California, Los Angeles, California 90089-0740, USA
† Department of Earth and Space Sciences, University of California, Los Angeles, California 90095, USA
‡ Jet Propulsion Laboratory, California Institute of Technology, Pasadena, California 91109, USA
§ Department of Earth Sciences and Institute of Tectonics, University of California, Santa Cruz, California 95064, USA
|| Institute for the Study of the Continents, Department of Geological Sciences, Cornell University, Ithaca, New York 14853, USA

The topography of tectonically active mountain ranges reflects a poorly understood competition between bedrock uplift and erosion. Dating of abandoned river-cut surfaces in the northwestern Himalayas reveals that the Indus river incises through the bedrock at extremely high rates (2–12 mm yr^{-1}). In the surrounding mountains, the average angles of hillslopes are steep and essentially independent of erosion rate, suggesting control by a common threshold process. In this rapidly deforming region, an equilibrium is maintained between bedrock uplift and river incision, with landsliding allowing hillslopes to adjust efficiently to rapid river downcutting.

THE interactions between tectonic and erosional processes are poorly understood in most actively deforming mountain belts. Mountainous topography results from the imbalance between the upward flux of bedrock into a region due to tectonics and the outward mass flux due to denudation by either tectonic (extensional faulting) or surface (fluvial, glacial and hillslope) processes. Analysis of tectonically active landscapes therefore requires quantification of topographical characteristics, together with documentation of rates of bedrock uplift, tectonic extension and geomorphic processes. Beyond coastal areas where sea level provides a reference surface, however, it is notoriously difficult to quantify bedrock uplift[1,2]. Key geomorphic controls, such as rates of river incision or hillslope erosion, are often unknown, as are data constraining the relationships between rates of surface processes and topographic descriptors of the landscape, such as relief or slope angles.

Here we focus on the middle gorge of the Indus river near Nanga Parbat in northern Pakistan, in the northwestern Himalayas (Fig. 1). The north–south-trending Nanga Parbat/Haramosh axis (NPHA) has long been hypothesized to be an area experiencing rapid bedrock uplift during Quaternary times[3]. The suture zone (main mantle thrust, or MMT in Fig. 1) between the Indian subcontinent and the southern margin of the Kohistan–Ladakh terrane is distinctly warped around the NPHA. Bounding the western margin of the NPHA, the Raikot fault[4] is the only identified large-scale active fault in the region. The highest stream-gradient indices of any important Himalayan river occur where the Indus crosses the NPHA[5]. Apatite and zircon fission-track ages[6,7] and numerous radiometric dates[8–11] clearly indicate that the NPHA (Fig. 1) has experienced rapid cooling, which has been interpreted to result from high bedrock uplift and denudation rates[6,7,10,12]. The strong contrasts in radiometric ages between the NPHA and adjacent regions make this an obvious site in which to explore the reaction of topography to contrasts in tectonic deformation rates.

We quantify here key interactions between tectonic and geomorphic processes along the Indus. On the basis of cosmogenic radionuclide exposure ages of abandoned river-cut terraces, we document some of the highest known rates of bedrock incision (2–12 mm yr^{-1}). We calculate rates of long-term denudation from published bedrock cooling ages, and assess bedrock uplift by combining incision rates with reasonable schemes for the evolution of the longitudinal profile of the Indus. The distribution of hillslope angles is both remarkably similar among contrasting regions and apparently independent of rates of denudation or river incision. Steep mean slope angles suggest a landscape poised near the threshold for landsliding involving the bedrock. Downcutting by large rivers roughly balances regionally variable rates of bedrock uplift. Throughout the reach of the Indus that we have studied, the rate of bedrock incision exceeds 2 mm yr^{-1} and drives down the toes of the adjacent slopes so rapidly that they adjust most efficiently through landsliding.

Bedrock incision rates

When a river cuts laterally into a bedrock valley wall, it carves a bench, or strath. Subsequent vertical incision causes abandonment of the strath. If the time since abandonment and the height of the strath above the valley bottom are known, a mean rate of river incision can be determined. Numerous straths are remarkably well preserved at heights ranging from 10 to 400 m or more above the Indus. Cut into metamorphic and igneous bedrock and lacking downstream continuity, many straths appear to be nearly pristine surfaces, 10 to 200 m wide, whose characteristics mimic those of river-worn surfaces along the modern channel. Straths that have experienced little erosional modification since abandonment are identified by streamlined bedrock knobs protruding 1–10 m above the mean strath surface, which is also sculpted, potholed and polished. Unlike straths in many other areas, alluvial mantles either were never present or were swept off many Indus straths. Although some straths have been buried by ancient landslides, such straths can usually be identified and were not sampled.

We collected bedrock samples near the outer edge of individual straths along the Indus between the Raikot fault and the Skardu basin (Fig. 1) for exposure-age dating using cosmogenic ^{10}Be and ^{26}Al. To take advantage of known ^{10}Be and ^{26}Al production rates in quartz[13], quartz-rich samples were dated[14]. All ^{10}Be/^{9}Be and ^{26}Al/^{27}Al measurements were made by accelerator mass spectrometry at Lawrence Livermore National Laboratory. Reported ages (Table 1) are corrected for altitude, latitude and exposure geometry[13,15]. Cited errors (2σ) include propagation of all

measurement uncertainties; production-rate uncertainties are excluded from the error analysis. All measured ^{26}Al ages (five samples) were concordant with ^{10}Be ages on the same sample (Table 1). This concordance and the fact that the measured ratios of $^{26}Al/^{10}Be$ are equal to the known production-rate ratios of these isotopes suggest that these surfaces have not experienced significant erosion or burial[16] and reinforce our interpretation of the sampled bedrock terraces as pristine strath surfaces. Four straths yielded consistent ages from two separate sites tens of metres apart (straths 1, 3, 4 and 7), whereas two surfaces (straths 2 and 6) have contrasting ages from separate sites (Table 1). Inconsistent ages can result from cosmic-ray screening of a site by an overlying boulder or from sampling a surface that either was more recently exposed because of spalling or which stood significantly above adjacent eroding surfaces. We have little field evidence for any of these explanations. In each case of mismatched ages on a single strath, one age is consistent with another dated strath nearby, and we have used this age in our interpretations.

Straths ranging from 65 to 410 m above the height of the Indus at low discharge yielded exposure ages spanning a range from about 4 to 68 kyr (Table 1). Making the assumption that the interval of strath formation was short in comparison to the time since abandonment by the Indus, we combined the mean exposure age of each strath and its height above the river to yield an average bedrock incision rate. High-water lines from annual floods are typically present 10 m or more above the low-stage discharges that prevailed during our sampling. Exposure ages on rock surfaces 1–5 m above the low-stage Indus yield ages indistinguishable from our process blank and indicate active erosion of these surfaces. For incision calculations, we assume that active river erosion at timescales of several decades occurs up to 20 m above low-water levels. Thus, the calculated rates are conservative, minimum rates. At the only site where we have dated vertically juxtaposed straths (straths 5 and 6), they yield consistent incision rates. Indus incision rates (Table 1) range from $\sim 2\,mm\,yr^{-1}$ to $12\,mm\,yr^{-1}$ between the Skardu basin and the Raikot fault (Fig. 2). These rates are some of the highest sustained bedrock incision rates that have been documented anywhere in the world. There is, moreover, a distinct spatial pattern of incision rates. At all sampled localities within and adjacent to the NPHA, incision rates are high, displaying maximum rates of $8–12\,mm\,yr^{-1}$ (Fig. 2).

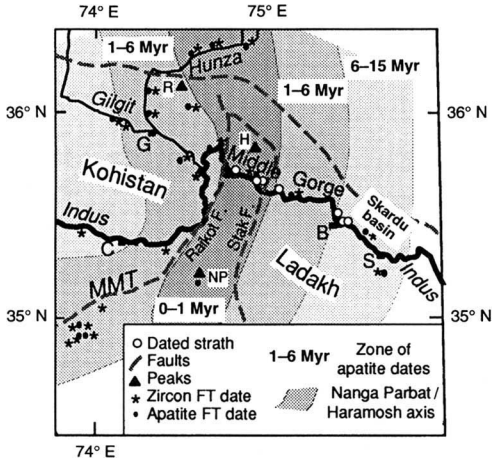

FIG. 1 Map of the Nanga Parbat region of the Indus river catchment showing main tributary rivers, dated straths in the middle gorge of the Indus, apatite and zircon fission-track (FT) dates, zones of contrasting apatite fission-track dates (indicated by different shading), and main faults (F). The youngest apatite dates correspond with the Nanga Parbat/Haramosh axis (darkest shading). B, Bashu; C, Chilas; G, Gilgit; H, Haramosh; MMT, main mantle thrust; NP, Nanga Parbat; R, Rakaposhi; S, Skardu.

Fifty kilometres to the east, rates seem to diminish slightly (to 5–$7\,mm\,yr^{-1}$: strath 3), whereas less than 10 km farther east, rates decrease abruptly to $2–3\,mm\,yr^{-1}$. Here, across a horizontal distance of a few kilometres there is a 3-fold change in bedrock incision rates (Fig. 2).

Long-term denudation

Whereas cosmogenic radionuclide exposure ages define short-term incision rates, they do not reveal the persistence or variability of these rates over longer time intervals. Long-term denudation rates can be estimated from radiometric cooling ages, if that cooling is the result of the upward motion of rock with respect to the Earth's surface ('bedrock exhumation'[1]). The cooling age represents the time since a given mineral in a rock sample was at or above the mineral closure or annealing temperature. With a known or assumed geothermal gradient of increasing temperature with depth, one can estimate a depth below the surface at which the sample had to be for that temperature. The approximate long-term denudation rate is then the depth or thickness of rocks removed divided by the cooling age. Conservative estimates of annealing temperatures ($\sim$120 and 210 °C for rapidly cooled apatite and zircon, respectively[7,17,18]) are used here, because they minimize the calculated denudation rate. Rapid cooling rates indicated by many young ages may warrant both higher annealing temperatures (150 and 240 °C)[12,19] and faster estimated denudation rates.

Past geothermal gradients and any temporal changes in those gradients are unknown. In nearby, but more slowly denuding Kohistan (Fig. 1), an early Miocene gradient of $\sim 40\,°C\,km^{-1}$ is definable on the basis of fission-track data.[7] An appropriate upper limit to the geothermal gradient of $\sim 60\,°C\,km^{-1}$ in areas of very rapid Pleistocene denudation[6] is suggested by pressure–temperature data and co-existing $^{40}Ar/^{39}Ar$ ages ($\sim$1 Myr on biotite) from high elevations on Nanga Parbat[10]. Given calculated denudation rates of $\geqslant 1\,mm\,yr^{-1}$ during the past 2 Myr (Fig. 2) in most of the study area, a likely lower limit of $35\,°C\,km^{-1}$ would be expected to result from advection and compression of isotherms in response to denudation[20]. We therefore use gradients of $35\,°C\,km^{-1}$ and $60\,°C\,km^{-1}$ to place probable bounds on long-term denudation rates.

The apatite fission-track dates[6,7] yield bedrock cooling rates ranging from $>250\,°C\,Myr^{-1}$ in the NPHA to $<15\,°C\,Myr^{-1}$ near Skardu. Comparisons of long-term denudation rates based on these dates with incision rates determined using cosmogenic nuclides for nearby strath surfaces (Fig. 2) indicate, first, that high denudation rates are associated with high incision rates across the NPHA; second, that the eastern limits of the zones of high denudation and of high bedrock incision rates are marked by abrupt, 2-to-4-fold decreases in calculated rates; third, given the uncertainties in past geothermal gradients, that long-term denudation rates during the past 0.5–1 Myr across the NPHA are strikingly similar to late Pleistocene incision rates; and fourth, that the zone of rapid bedrock incision seems to be broader than the zone of rapid long-term denudation. The greater breadth of the zone of rapid incision (Fig. 2) creates a mismatch of rates for $\sim$50km upstream of the NPHA and suggests that denudation rates in this region may have accelerated during latest Quaternary times. Overall, denudation rates similar to those defined by the incision data are likely to have persisted for 0.5 Myr or more within the NPHA, during which time $\sim$2–4 km of bedrock would have been removed from the NPHA itself. Whereas such denudation rates have been estimated previously[7,10,12], we are now able to compare them directly with bedrock incision rates for the same geographical localities.

Cooling rates based on zircon fission-track dates are only half as rapid as those determined from apatite dates on the same or nearby samples[6,7], except in the Skardu basin, where rates are uniformly slow ($< 15\,°C\,Myr^{-1}$). This difference in cooling rates could result from accelerating denudation rates or Pleistocene steepening of the geothermal gradient. Some combination of the

TABLE 1 ^{10}Be and ^{26}Al exposure ages for strath terraces in the Middle Gorge of the Indus river

Strath no.	Sample no.	Distance upstream (km)	Altitude (m)	Height above river (m)	^{10}Be concentration (10^6 atoms per g qz)	^{10}Be age (kyr)	^{26}Al concentration (10^6 atoms per g qz)	^{26}Al age (kyr)	Averaged strath age (kyr)	Incision rate (mm yr^{-1})*
1	93-20	133	2,235	185	1.43 ± 0.16	60 ± 7	n.m.	n.m.	61 ± 6	2.7 ± 0.4
	93-22	133	2,233	183	1.53 ± 0.42	67 ± 19	n.m.	n.m.		
2	93-23	131	2,198	148	1.49 ± 0.14	65 ± 6	9.24 ± 0.70	68 ± 5	67 ± 4	1.9 ± 0.2
	93-25	131	2,195	145	0.75 ± 0.05	(32 ± 2)	n.m.	n.m.		
3	93-17	124	2,082	65	0.15 ± 0.01	7 ± 1	n.m.	n.m.	7 ± 1	6.5 ± 1.8
	93-19	124	2,082	65	0.17 ± 0.04	8 ± 2	0.92 ± 0.28	7 ± 2		
4	93-29	81	1,850	70	0.13 ± 0.03	7 ± 2	n.m.	n.m.	6 ± 1	7.8 ± 2.6
	93-30	81	1,840	65	0.08 ± 0.03	4 ± 2	n.m.	n.m.		
5	95-31	69	2,150	410	0.76 ± 0.06	32 ± 2	4.50 ± 0.65	32 ± 5	32 ± 2	12.1 ± 0.9
6	93-96	68	1,883	155	0.24 ± 0.13	12 ± 7	1.70 ± 0.36	15 ± 3	14 ± 3	9.6 ± 2.3
	93-38	68	1,882	154	0.55 ± 0.05	(29 ± 3)	2.93 ± 0.32	(25 ± 3)		
7	93-39	52	1,675	80	0.12 ± 0.02	8 ± 1	n.m.	n.m.	7 ± 1	8.9 ± 2.2
	93-40	52	1,675	80	0.80 ± 0.02	5 ± 1	n.m.	n.m.		

All uncertainties are 2σ values. Values listed in parentheses are not used to calculate average strath age. n.m., not measured.
* Rate is calculated assuming active erosion up to 20 m above low-discharge levels of the Indus. Incision rate error is calculated using uncertainty in average age and a 5-m uncertainty in elevation.

two seems likely. Irrespective of possible changes in the geothermal gradient, when compared with the apatite and incision data, the zircons in the NPHA also yield the highest rates of denudation and comparable contrasts of high-to-low rates across the eastern NPHA (Fig. 2). Even if the geothermal gradient increased from 35 to 60 °C km^{-1} at all sites between the early and middle Pleistocene, there is evidence for modest (20–50%) acceleration of denudation rates at this time. Comparisons of rates based on apatite versus strath ages suggest the accelerating trend has persisted into late Pleistocene times (Fig. 2).

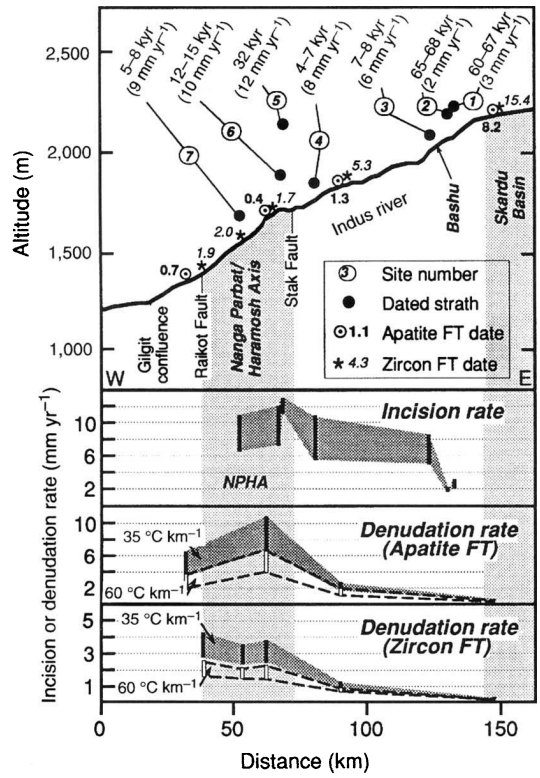

FIG. 2 Longitudinal profile of the Indus river from near its confluence with the Gilgit river, across the NPHA and middle gorge to the Skardu basin. The locations, height above the Indus, ages, incision rates and numbers of dated straths are shown along with the location and ages of spatially associated fission-track dates[7]. Incision rates (with 2σ uncertainties) are highest in the NPHA (second panel). Between straths 2 and 3 near Bashu, there is a roughly 3-fold increase in incision rates. Across the eastern edge of the NPHA (corresponding roughly to the Stak fault zone), a comparable change occurs in denudation rates (lower panels) derived from apatite and zircon fission-track ages. Ranges of denudation rates (2σ) are depicted for 35 °C km^{-1} and 60 °C km^{-1} geothermal gradients. Note change in vertical scale for zircon data.

Calculation of bedrock uplift

The distinctive gradient in incision rates within the upper part of the middle Indus gorge (straths 1–3: Fig. 2) cannot be attributed to differences in erodability of the bedrock within the NPHA of the Ladakh terrane (Fig. 1), because both comprise highly resistant igneous and metamorphic rocks. Rather, contrasting rates seem to be driven by differential bedrock uplift near Bashu (Fig. 3*a*). We attempt here to constrain both differential uplift and absolute bedrock-uplift rates.

If we assume that incision rates defined at each site have persisted for at least 65 kyr (the approximate age of the oldest dated straths), then the height above the present Indus of a strath formed 65 kyr ago can be predicted by extrapolating short-term incision rates back through time. Thus, for the 32-kyr-old strath (strath 5) which is currently 410 m above the Indus, a 65-kyr-old strath in that location would be 830 m above the modern river. By connecting the projected positions of these straths, the deformed longitudinal profile of the Indus at ~65 kyr can be reconstructed (Fig. 3*a*). The 32-kyr-old strath defines the lowest permissible altitude for this profile within the NPHA. Comparison of the reconstructed and modern Indus profiles reveals pronounced differential bedrock uplift near Bashu, downstream divergence of the longitudinal profiles, and low-gradient reconstructed 65-kyr profile, whose western half is 500–800 m above the modern Indus.

The far more difficult task of defining bedrock uplift with respect to the geoid[2] can be examined initially near Bashu (Fig. 3*a*). Given the young radiometric ages nearby[7,8,12], it is highly unlikely that bedrock is subsiding with respect to the geoid. We assume conservatively that there has been no bedrock uplift in the area of the 65-kyr strath upstream of Bashu (that is, bedrock here was fixed with respect to the geoid) and that the Indus has incised steadily after abandoning the 65-kyr strath (Fig. 3*b*). This permits us to estimate the height of the Indus at ~7 kyr upstream of Bashu and to compare it with the surface at the same age 7–9 km downstream (strath 3). The river gradient at 7 kyr is unknown, but it certainly was more than 0° and probably was no steeper than the modern gradient. The altitudinal offset of the 7-kyr strath with respect to these two gradient limits defines bedrock uplift ranging from 2 to 5 mm yr^{-1} for the downstream region (Fig. 3*b*). It seems unlikely, however, that the gradient of the Indus was negligible throughout this reach, because that requires improbably steep gradients farther downstream. If both the elevation and gradient of the Indus River at 7-kyr were about the same as today, then

incision by the Indus is keeping pace with bedrock uplift. This latter picture implies that the longitudinal profile of the Indus in this region could be regarded as a fixed reference frame against which the vertical movement of bedrock could be measured.

Fluvial incision into bedrock is driven by specific stream power[21–23], which is proportional to the product of slope and discharge and is inversely proportional to river width. Because the middle gorge has a catchment area of $>10^5$ km^2 and is >600 km from the Indus headwaters, there is considerable discharge through it (summer flows are typically >3,000 m^3 s^{-1}). Moreover, no significant tributaries join the Indus in the middle gorge. The variation in the Indus gradient throughout this reach, therefore, dictates the pattern of stream power. That the Indus currently displays its maximum gradient (Fig. 3*c*) in and around the NPHA[5] implies that the longitudinal profile of the Indus may be in rough equilibrium with the bedrock uplift pattern.

Although a fixed position with respect to the geoid is probably not realistic for many rivers in actively deforming areas, we suggest that it is appropriate here during the past 0.5–1 Myr. Given the similar magnitude within the NPHA of both denudation rates and incision rates (Fig. 2), many kilometres of rock must have been eroded from the NPHA during the Quaternary. Any sustained mismatch between the rates of incision and bedrock uplift would result in considerable perturbations in the longitudinal profile of the Indus (Fig. 3*c*). It is, therefore, important to assess the evidence for any such perturbations.

If incision rates exceed bedrock uplift rates in the NPHA, the Indus will lower its elevation within the NPHA and necessarily lower its gradient below this reach. Unless the Indus also becomes narrower (the opposite of what is observed in the gentler reaches), the lowered gradient generates a negative feedback which decreases both the specific stream power and the rate of incision until a new balance is attained between gradient, incision rate and bedrock uplift rate. Given that the study area is >1,200 km from the mouth of the Indus, and that the river traverses 400 km of mountainous terrain after crossing the NPHA, the Indus simply cannot lower its downstream gradient too much. For example, if present incision rates were sustained for 100 kyr in the face of no bedrock uplift (Fig. 3*c*), the Indus would be nearly below sea level in the study area.

If, on the other hand, rates of bedrock uplift were greater than rates of incision across a zone of rapid differential uplift, the slope of the Indus would decrease with time across the uplift. The gradient downstream of the uplifting region, however, would increase, promoting accelerated incision. If the mismatch across the uplift persisted, the river could become tectonically dammed and/or have its flow reversed. To maintain an oceanward gradient, an upstream reach of the river must aggrade and/or be uplifted at a rate equal to the difference between uplift and incision downstream. A rapid pulse of aggradation did occur in the Skardu basin, immediately above the middle gorge, during the early Pleistocene[24,25] and may reflect a transient response to such a mismatch of incision rates with newly accelerated bedrock uplift rates[26]. There is, however, little evidence for extensive aggradation along the upper reaches of the Indus, where calculated denudation rates[27] are ~40 times less than those in the NPHA. We cannot eliminate the possibility that the entire Indus drainage upstream of the NPHA experienced bedrock uplift during a part of the Quaternary at a rate nearly equal to the difference between uplift and incision rates at the NPHA. But given the present upstream elevation of the Indus (~3,000 m near Leh, >300 km upstream) and its large distance from the ocean (~1,500 km at Leh), the low Neogene denudation rates described along its upstream course[7,27], and the likely rates of bedrock incision as determined from stream power calibrated against our incision data[26], it is unlikely that the elevation of the Indus upstream of the study area has increased by >1 km during the past 1 Myr. Because this represents <25% of the documented denudation across the NPHA, we conclude that

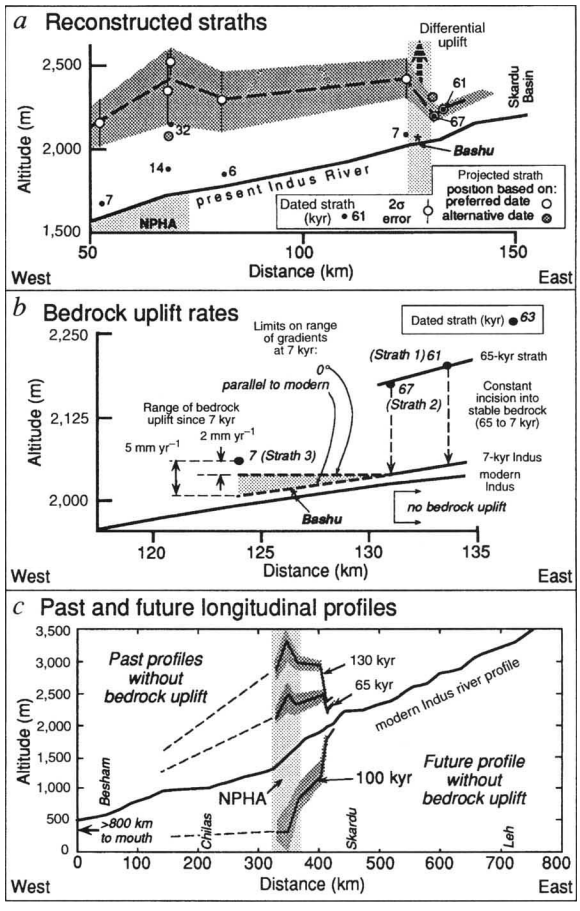

FIG. 3 *a*, Reconstruction of strath geometries along the middle Indus gorge. Extrapolation of site-specific incision rates (assumed constant during the past 65 kyr) define expected present-day altitudinal positions of 65-kyr-old straths (dashed line, with 2σ error). Strong warping of reconstructed Indus course at 65 kyr ago (stippled area) illustrates clear differential uplift of the downstream reach. Note that if no bedrock uplift is assumed, the Indus in the NPHA region would have been ~1 km above its present elevation less than 0.1 Myr ago. This would require very steep downstream gradients and improbable upstream river profiles. *b*, Two interpretations of bedrock uplift near Bashu, assuming no bedrock uplift further than 131 km upstream (strath 2) and constant incision between 65 and 7 kyr ago. The downstream strath at 7 kyr (strath 3) is altitudinally above the calculated river position upstream at 131 km. The amount and rate of bedrock uplift of strath 3 depends on the assumed gradient downstream of 131 km. A minimum bedrock uplift rate of 2 mm yr^{-1} results from assuming an improbable, flat gradient. If the gradient were parallel to the modern, the bedrock uplift rate would be $\geqslant$5 mm^{-1}. *c*, Comparison of the longitudinal profile of the modern Indus with profiles that would be predicted if there were no bedrock uplift, but if present incision rates persisted into the past or future. The steepest gradient of the modern Indus occurs in and near the NPHA, where incision rates are highest. At 65 kyr ago, there would have been a very gentle gradient across the NPHA and a much steeper downstream gradient than at present without bedrock uplift. Additional extrapolation to 130 kyr ago yields an even steeper downstream gradient (through an area with relatively old cooling ages: Fig. 1) and predicts a reversal of dip of the river profile across the NPHA.This is a highly unlikely geometry for the river at that time, but is the expected configuration for straths of that age, if there were no bedrock uplift. If present incision rates were to continue 65 kyr into the future without bedrock uplift, the river would be near sea level in the NPHA: clearly another improbable geometry. Note that, if the course of the Indus upstream of Skardu has been raised 1 km during the Quaternary, this would require a gentle (and unlikely) gradient across the NPHA at 1 Myr ago. These examples indicate that bedrock uplift and incision must be nearly in balance across the middle Indus gorge.

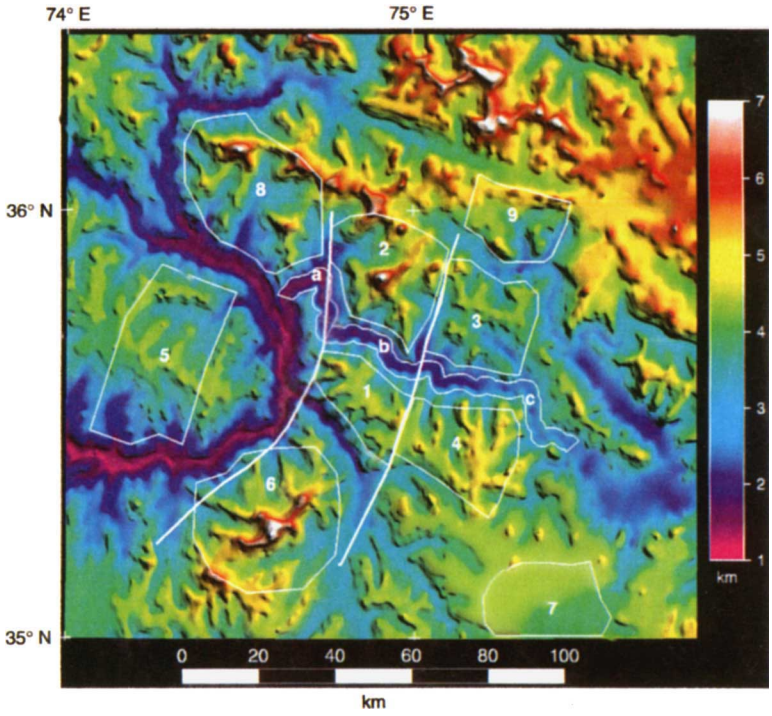

FIG. 4 Digital topography of the Nanga Parbat region of northern Pakistan, derived from public-domain data on the *Digital Chart of the World*, which has ~1% of the resolution of the 3-arcsecond data used in the topographic analyses. Altitudes range from 1 to >8 km. Areas analysed for slope distributions (Fig. 5) are either 4-km-wide swaths along the Indus river or extensive mountainous (areas 1, 2, 3, 6, 8 and 9) or plateau-like regions (areas 4, 5 and 7) next to it, shown as white polygons. Nanga Parbat is in region 6, Haramosh in region 2, Rakaposhi in region 8, the Gamugah surface in region 5, and the Deosai Plateau in region 7. The middle gorge of the Indus flows from swath **c** through swath **a**. The approximate traces of the Raikot and Stak faults are shown (thick white lines).

bedrock uplift and incision rates have been nearly balanced across the NPHA during much of the past 1 Myr, that the longitudinal profile of the Indus is roughly fixed with respect to the geoid, and that incision rates therefore provide a reasonable proxy for bedrock uplift rates (±25%) during the Quaternary in the study area.

Responses to differential uplift

It has often been argued that high rates of bedrock uplift and denudation should be correlated with steep slope angles[28], because hillslope erosion rates are strongly slope-dependent[23,29,30]. In the Nanga Parbat region, excellent opportunities exist to test these concepts at large scales, because the incision and radiometric data define regions of sharply contrasting rates of denudation (Fig. 2), and because digital topographic data permit quantification of regional topographic characteristics.

We have analysed a digital elevation model (DEM) with 3-arcsecond (~90-m) grid spacing[31]. Slope angles are defined using a 4 × 4-point window within which the slope of a best-fitting plane is calculated to the nearest 0.1°. The ~270 m size of the measurement window causes slopes to be underestimated, especially in areas where hillslopes have substantial curvature, such as across sharp ridges or valley bottoms. For each area analysed, ~10,000–40,000 slope determinations are collected into a histogram. The resultant slope distributions are sorted into 1° bins and then normalized by area to permit comparison between unequally sized areas.

We have analysed six mountainous regions that sample the contrasting zones of denudation, three plateau-like regions, and three 4-km-wide swaths centred along the Indus river where we have incision or denudation data (Fig. 4; note that Fig. 4 does not show the 3-arcsecond data). We analysed the mountains and the Indus valley separately in case large river valleys strongly perturb slope distributions.The summits of Nanga Parbat (8,126 m) and Haramosh (7,458 m) occur in the mountainous regions analysed within the NPHA. Rakaposhi (7,788 m) lies to the northwest of the NPHA (Figs 1 and 4) near the margins of a region whose fission-track dates[7] suggest denudation rates similar to the relatively low rates along the Indus upstream of the NPHA. No comparably high summits lie in the selected regions to the east of the NPHA. The plateau-like areas include the central Deosai Plateau, a mountainous area that encompasses one margin of the Deosai and the partially dissected 'Gamugah' surface (Fig. 4).

Remarkably, the distributions of slopes are essentially indistinguishable among different mountainous regions, despite significant differences in denudation rates (Fig. 5*a*). In each region, most slopes fall between 20° and 45°, and the mean slope angle is ~ 32 ± 2° (for 270-m windows). Some regions containing large valley glaciers, which typically have low gradients, have a secondary peak of low slope angles (~5°). The swaths along the Indus show similarly high mean slope angles (Fig. 5*b*). In fact, the highest mean slope angle (38°) among all areas analysed occurs along the largely unglaciated reach of the Indus with the highest incision and denudation rates. Whereas the central Deosai Plateau displays low mean slopes (~11°), more heavily dissected plateau remnants (Fig. 5*c*) show relatively high mean slopes (~26°). There are few radiometric ages to constrain directly the cooling or denudation histories of these plateaux. Most dates along their margins indicate cooling rates of 10–20 °C Myr^{-1} (ref. 7), about 10 times slower than in the NPHA.

Three key conclusions can be drawn from the slope analysis. First, outside the plateaux, slope angles are largely independent of, rather than correlated with[28], denudation or bedrock-uplift rates. Nor are they correlated with predominantly glaciated (mountain) zones rather than non-glaciated (valley-bottom) zones. Second, uniformly high mean slope angles among all areas (other than the plateaux) suggest that a common threshold controls them. Third, the data do not support at least one proposal for hillslope response to accelerated denudation: 'slope replacement' through the lengthening of steeper slopes at the expense of gentler slopes[28,32]. The histograms measure the area of each slope category, and, when one compares less rapidly with more rapidly denuding areas, the histograms do not reveal any significant shift in slope distributions due to substitution of steeper for gentler slopes.

DEM analysis and field observations indicate that bedrock-involved landsliding[33] is the dominant denudational process in these rapidly denuding mountains. It is also important that rivers of this region are generally underloaded with respect to sediment. They successfully remove detritus supplied to them by adjacent hillsides, and throughout most of the area, they are flowing on or near bedrock. The absence of significant quantities of stored

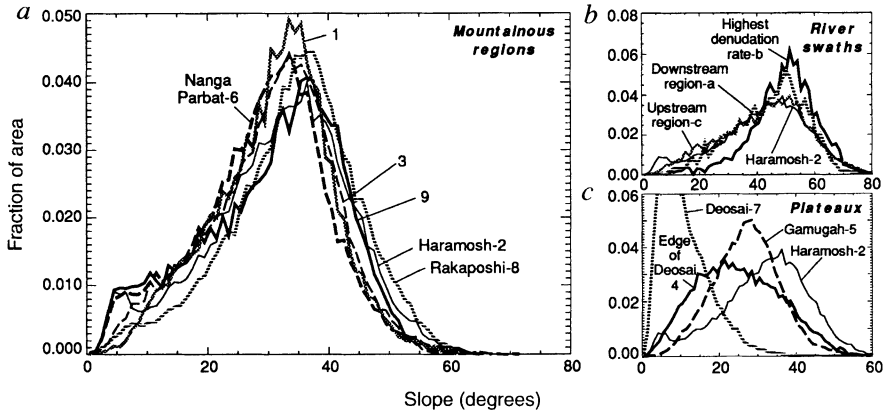

FIG. 5 *a*, Slope distributions in mountainous regions near Nanga Parbat, excluding plateaux. Each numbered histogram corresponds to a region defined on the DEM (Fig. 4). For comparison, all histograms are normalized by area. There are no significant differences between areas with high denudation rates in the NPHA (curves 1, 2 and 6) and areas with much lower denudation rates in adjacent regions. Although underestimated by the 90-m DEM, the mean slope angle for all areas is $32 \pm 2°$. *b*, Slope distributions for swaths ~4-km wide along the Middle Indus gorge. Highest mean slope angles (38°) occur in the region of most rapid incision (area **b**, Fig. 4) which also displays a smaller proportion of low slope angles than any of the other studied areas, possibly because of absence of significant glaciation in the valley bottom. Compared with the zone of the most rapid incision, lower slope angles are more prevalent in the downstream and upstream zones (**a** and **c**, respectively, Fig. 4), where valley widening has occurred at the expense of deepening. Histogram from Haramosh included for comparison with *a*. *c*, Distribution of slope angles for largely intact and partially dissected plateaux. The central Deosai plateau (area 7, Fig. 4) is dominated by low slopes, whereas those areas including parts of dissected plateaux (areas 4 and 5) show intermediate slope distributions compared to nearby mountainous zones. Histogram from Haramosh included for comparison with *a*.

sediment means that hillslope angles are not diminished by valley aggradation. Because most of the bedrock is extensively fractured, it lacks cohesion at the scale of large hillslopes. Thus, we interpret the typically high mean slope angles (32° using a 270 × 270-m window) as reflecting an average effective angle of internal friction which controls hillslope stability in this fractured bedrock.

Regardless of the controlling process of denudation, the similarity of slope distributions and the comparable mean altitudes (4,200–4,600 m) based on hypsometric (area versus altitude) analysis of all mountainous regions suggest homogeneous topographic characteristics, largely independent of denudation variations, in this landscape. The association of high river gradients with high rock-uplift rates implies a dynamic equilibrium in which bedrock uplift and incision are balanced through adjustments in stream power. Rates of denudation are sufficiently high that, even in areas with denudation rates of 1–2 mm yr^{-1}, the processes that typically affect soil-mantled slopes[34] (regolith production, creep and slope wash) are volumetrically unimportant. Instead, a threshold incision rate (perhaps 0.5 mm yr^{-1}) has been crossed, whereby rapid mass transfer through landsliding is the primary means by which the hillslopes adjust to changes in boundary conditions resulting from river incision at their toes. In this case, mean slope angles will be set by rock strength, and mean relief will be controlled by the spacing of large rivers[26]. Given that the spacing of large rivers is similar among different subregions, and that denudation calculations indicate at least several kilometres of bedrock erosion during the past 1 Myr throughout most of the area, attainment of dynamic equilibrium and uniform slope and altitudinal characteristics is perhaps not surprising. Herein, we have actually documented such an equilibrium for a very large-scale, high-relief and rapidly deforming part of the largest mountain range in the world.

A conceptual model for mountainous regions of variable but persistently high rates of bedrock uplift emerges from this analysis. Here, large rivers can attain equilibrium profiles wherein local fluvial gradients are adjusted until incision rates driven by stream power balance bedrock uplift rates. Large rivers become bedrock saws, fixed with respect to the geoid. Between rivers, bedrock rises towards denuding hillslopes whose rate of mass transfer to valley bottoms through landsliding is proportional to the incision rates of the great rivers. Because the threshold for landsliding is determined by fractured rock strength, the highest topography will develop either where rocks are less fractured or where large rivers are most widely spaced. To test or quantify this model, more data are needed on mass-flux rates through bedrock uplift and landsliding, on rates of river incision and glacial erosion, and on topographic variability within deforming regions. □

Received 18 August; accepted 27 December 1995.

1. Molnar, P. & England, P. *Nature* **346,** 29–34 (1990).
2. England, P. & Molnar, P. *Geology* **18,** 1173–1177 (1990).
3. Misch, P. *Festschrift zum 60. Geburtstag von Hans Stille*, 259–276 (Enke, Stuttagart, 1936).
4. Butler, R. W. H. & Prior, D. J. *Nature* **333,** 247–250 (1988).
5. Seeber, L. & Gornitz, V. *Tectonophysics* **92,** 335–367 (1983).
6. Zeitler, P. K., Johnson, N. M., Naeser, C. W. & Tahirkheli, R. A. K. *Nature* **298,** 255–257 (1982).
7. Zeitler, P. K. *Tectonics* **4,** 127–151 (1985).
8. Treloar, P. J. *et al. Tectonics* **8,** 881–909 (1989).
9. Zeitler, P. K., Chamberlain, C. P. & Smith, H. *Geology* **21,** 247–250 (1993).
10. Winslow, D. M., Zeitler, P. K., Chamberlain, C. P. & Hollister, L. S. *Geology* **22,** 1075–1078 (1994).
11. George, M., Reddy, S. & Harris, N. *Tectonics* **14,** 237–252 (1995).
12. Sorkhabi, R. B. *Nucl. Tracks Radiat. Meas.* **21,** 535–542 (1993).
13. Nishiizumi, K. *et al. J. geophys. Res.* **94,** 17907–17915 (1989).
14. Kohl, C. P. & Nishiizumi, K. *Geochim. cosmochim. Acta* **56,** 3583–3587 (1992).
15. Lal, D. *Earth planet. Sci. Lett.* **104,** 424–439 (1991).
16. Nishiizumi, K. *et al. Earth Surf. Proc. Landforms* **18,** 407–425 (1993).
17. Naeser, N. D., Naeser, C. W. & McCulloh, T. H. in *Thermal History of Sedimentary Basins: Methods and Case Studies* (eds Naeser, N.D. & McCulloh, T.H.) 157–180 (Springer, New York, 1989).
18. Harrison, T. M. *Nucl. Tracks* **10,** 329–333 (1985).
19. Naeser, C. W. *Nucl. Tracks* **5,** 248–250 (1981).
20. Stüwe, K., White, L. & Brown, R. *Earth planet. Sci. Lett.* **124,** 63–74 (1994).
21. Seidl, M. A. & Dietrich, W. E. *Catena Suppl.* **23,** 101–124 (1992).
22. Howard, A. D., Dietrich, W. E. & Seidl, M. A. *J. geophys. Res.* **99,** 13971–13986 (1994).
23. Rosenbloom, N. A. & Anderson, R. S. *J. Geophys. Res.* **99,** 14013–14029 (1994).
24. Cronin, V. S. in *Tectonics of the Western Himalayas* (eds Malineonico, L. L. Jr & Lillie, R. J.) 181–202 (Spec. Pap. 232, Geol. Soc. Am., Boulder, Colorado, 1989).
25. Cronin, V. S. & Johnson, G. D. in *Himalaya to the Sea Geology, Geomorphology and the Quaternary* (ed. Schroder, J. F. Jr) 91–107 (Routledge, London, 1993).
26. Anderson, R. S., Dick, G. S. & Densmore, A. *Geol. Soc. Am. Abstr. Prog.* **26,** 238–239 (1994).
27. Sorkhabi, R. B. *et al. Proc. Indian Acad. Sci. (Earth planet. Sci)* **103,** 83–97 (1994).
28. Penck, W. *Morphological Analysis of Landforms* (Macmillan, London, 1953).
29. Hanks, T. C., Bucknam, R. C., LaJoie, K. R. & Wallace, R. E. *J. geophys. Res.* **89,** 5771–5790 (1994).
30. Dietrich, W. E., Wilson, C. J., Montgomery, D. R. & McKean, J. *J. Geol.* **101,** 161–180 (1993).
31. Fielding, E. J., Isacks, B. L., Barazangi, M. & Duncan, C. *Geology* **22** , 163–167 (1994).
32. Carson, M. A. & Kirby, M. J. *Hillslope Form and Process* (Cambridge Univ. Press, Cambridge, 1972).
33. Shroder, J. F. Jr, Khan, M. S., Lawrence, R. D., Madin, I. P. & Higgins, S. M. in *Tectonics of the Western Himalayas* (eds Malinconico, L. L. Jr & Lillie, R. J.) 275–294 (Spec. Pap. 232, Geol. Soc. Am., Boulder, Colorado, 1989).
34. Dietrich, W. E., Wilson, C. J., Montgomery, D. R., McKean, J. & Bauer, R. *Geology* **20,** 675–679 (1992).

ACKNOWLEDGEMENTS. Support for this research was provided by the National Science Foundation, National Geographic Research and the National Aeronautics and Space Administration. We thank J. Vergés and J. Khan for assistance with field work and logistics, B. Isacks for discussions and contributions to the DEM analysis, K. Hodges, A. Howard and M. Seidl for reviews, M. Caffee, R. Finkel and J. Southon for assistance with the cosmogenic nuclide analyses at Lawrence Livermore National Laboratory, Earth Resource Mapping for an educational grant and Sun Microsystems for donating a graphics tower.